WATER AND THERMAL DIFFUSIVITY IN A LIPID-WATER SMECTIC PHASE

WINSTON K. CHAN AND PETER S. PERSHAN, *Division of Applied Sciences, Harvard University, Cambridge, Massachusetts 02138 U.S.A.*

ABSTRACT We report the first application of light scattering to measurement of the hydrodynamic relaxation of inhomogeneities in water concentration within a multilamellar, or smectic A, phospholipid water system (dipalmitoyl phosphatidyl choline). Although the relaxation process in the multilamellar phase is different from the diffusion process in liquid phases, the relaxation rate can be described in terms of a diffusion coefficient. For diffusion parallel to the lamellae, diffusion coefficients ranging from 8×10^{-7} to 2×10^{-5} cm^2/s were measured over a range of temperature and water concentrations. We describe a model that expresses the diffusion coefficient in terms of the chemical potential for water inside the multilamellar phase and the effective thickness of a "free water zone." The deduced thickness of this free water zone is in good agreement with estimates from X-ray diffraction results. The activation energy for the diffusion process is also deduced from the data, and is found to decrease monotonically with increasing water concentration. We also found the thermal diffusivity to be about 10^{-3} cm^2/s, with only a weak temperature and water concentration dependence.

The experimental technique is a new version of forced Rayleigh scattering. The method uses the phase information of the scattered light to improve the ability to detect weak signals. Experimental details are reported.

INTRODUCTION

Basic information concerning the physical properties of membrane lipids has been obtained from studies on model systems such as phospholipid monolayers, bilayers, vesicles, and multilamellar phospholipid-water phases (1, 2). The last of these forms well-defined liquid crystalline phases that can be obtained as macroscopically aligned samples amenable to the same experimental techniques applied profitably to crystals and other liquid crystals (3). This paper describes the first experimental study of the hydrodynamic relaxation of nonuniform water concentrations in an aligned smectic-A sample of dipalmitoyl phosphatidyl choline (DPPC) as a function of water concentration and temperature. The results to be described below include the diffusion constant for water and an independent measure of the fraction of free to bound water within this liquid crystalline phase.

A part of the phase diagram for DPPC-water is shown in Fig. 1 (1, 4–7). The regions

---

Dr. Chan's current address is: School of Applied and Engineering Physics, Cornell University, Ithaca, N.Y. 14853.

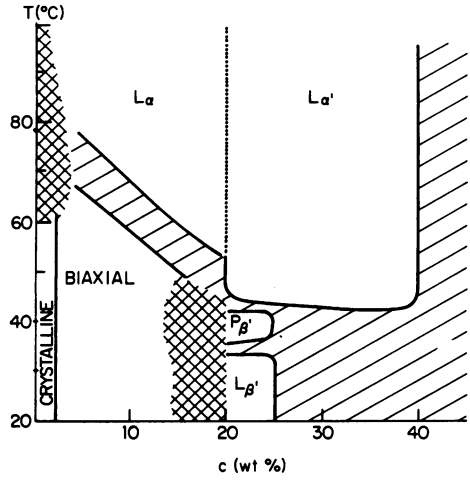

FIGURE 1 Schematic illustration of the phase diagram for DPPC-water. Diagonal lines indicate two-phase regions and cross-hatching indicates regions where the phase diagram is not determined.

marked L_α and $L_{\alpha'}$ are referred to as smectic A in the liquid crystal literature (3). These regions are usually described as consisting of planar lipid bilayers separated by water layers whose thickness depends primarily on water concentration. Actually the water intercalates between and around the polar head group of the DPPC molecule and it is not possible to distinguish clearly between the water layer and the polar head group region (5). The DPPC molecule itself is free to rotate about an axis normal to the bilayer plane and the system is macroscopically uniaxial. X-ray diffraction studies confirm that the smectic-A phase is periodic along the symmetry axis with a repeat distance of the order of ~50–60 Å (1, 4). There is no long-range order perpendicular to the symmetry axis and diffraction studies indicate only liquid-like structures within the bilayer.

As a result of the one-dimensional periodicity normal to the bilayer, water diffusion parallel to the bilayer is physically different from water diffusion in an unstructured or isotropic system. Brochard and de Gennes described one specific model that illustrates the difference (8). For example, in the lamellar system an increase in the local water concentration demands either that the combined thickness of the water and lipid layer increase or that the lipid layer be compressed to accommodate the extra water. Since the experiment to be described below maintains the combined thickness fixed, an increase in local water concentration induces elastic-like compression of the lipid layer, which provides the restoring force to return the system to uniform water concentration. In contrast to this, for an isotropic system, the restoring force opposing concentration fluctuations is predominantly entropic. This is also the case for diffusion of small concentrations of a marker molecule such as tritiated water in the remaining water of the smectic system. A nonuniform concentration of tritiated water need not produce the elastic deformations mentioned above, because the sum of normal and tritiated water concentrations can be maintained uniform.

In the experiment described below, we first produce a sinusoidal variation in the local temperature and water concentration of the form $\cos(q_0 x)$, where the x direction is in the bilayer plane. Since the index of refraction n is a function of both these variables, the effect is to produce a sinusoidal variation $\delta n \sim \cos(q_0 x)$, which acts as a diffraction grating. The driving force that established the sinusoidal variation δn is turned off and the relaxation of δn back to zero is monitored by observing the decay in amplitude of light diffracted by the grating. This can be related back to the relaxations of the temperature and water concentration variations. Under Hydrodynamic Theory we will review some of the principle theoretical results for the hydrodynamic relaxation of temperature and concentration inhomogeneities and show that there are two decay times of the form $\tau_i^{-1} = \Gamma_i q_0^2$, $i = 1, 2$. One of these corresponds to thermal diffusivity and is two to three orders of magnitude faster than the second, which corresponds to the diffusion of water. The experiment itself, a variation of the "forced Rayleigh technique," will be described next (9–12). Details of the sample preparation, the experimental results, the analysis of the data, and the conclusions that can be drawn from these measurements will be discussed below.

HYDRODYNAMIC THEORY

A general hydrodynamic theory applicable to the smectic-A phase of DPPC-water samples has been developed by Martin et al. (13) and predictions specific to this system have been made by Brochard and de Gennes (8). For our purposes it is sufficient to know that basic theoretical arguments obtain the following differential equations to describe slow relaxation behavior of the DPPC-water system. Assuming the only spatial variations are along the x direction in the bilayer planes,

$$\rho \partial c/\partial t = \zeta \partial^2 \bar{\mu}/\partial x^2 + \gamma T^{-1} \partial^2 T/\partial x^2 \tag{1}$$

$$\rho T \partial S/\partial t = \gamma \partial^2 \bar{\mu}/\partial x^2 + \kappa \partial^2 T/\partial x^2, \tag{2}$$

where c = the weight fraction of water to total sample, ρ = the sample density, S = the entropy per unit mass, T = the temperature, and $\bar{\mu} = (\mu_1/M_1) - (\mu_2/M_2)$. The quantities μ_1, M_1 and μ_2, M_2 are the chemical potentials and molecular masses of water and DPPC, respectively. The three constants ζ, γ, and κ are phenomenological dissipative parameters.

To obtain a complete solution for the relaxation behavior of this system, one expands $\bar{\mu}$ and S as power series in the deviations δc and δT from equilibrium values. In the limit of small deviations δc and δT, a linear approximation is adequate, and on substitution of

$$\delta \bar{\mu} = (\partial \bar{\mu}/\partial c)_{T,P} \delta c + (\partial \bar{\mu}/\partial T)_{c,P} \delta T, \text{ and} \tag{3}$$

$$\delta S = (\partial S/\partial c)_{T,P} \delta c + (\partial S/\partial T)_{c,P} \delta T \tag{4}$$

into Eqs. 1 and 2, it is straightforward to solve for the characteristic decay times with initial conditions:

$$\delta c(x, 0) = \delta c_0 \exp(i q_0 x), \tag{5}$$

$$\delta T(x, 0) = \delta T_0 \exp(i q_0 x). \tag{6}$$

The initial values δc_0 and δT_0 can be found by assuming a sinusoidal heat source applied for a time interval ending at $t = 0$ to a system that initially is spatially uniform. Specific values for δc_0 and δT_0 are not needed for our discussion. The solution has the form:

$$\delta c(x, t) = (A_{11} e^{-t/\tau_1} + A_{12} e^{-t/\tau_2}) e^{iq_0 x}, \tag{7}$$

$$\delta T(x, t) = (A_{21} e^{-t/\tau_1} + A_{22} e^{-t/\tau_2}) e^{iq_0 x}, \tag{8}$$

where the A_{ij} and the τ_i are involved functions of the three dissipative parameters ζ, γ, and κ, as well as three thermodynamic derivatives: the specific heat $T(\partial S/\partial T)_{c,P}$, the derivative $(\partial \bar{\mu}/\partial c)_{T,P}$ and the cross term $(\partial \bar{\mu}/\partial T)_{c,P} = -(\partial S/\partial c)_{T,P}$. It is not difficult to show that both τ_1 and τ_2 have the form $\tau_i^{-1} = \Gamma_i q_0^2$. The amplitude of the diffraction grating should thus decay as the sum of two exponentials, with time constants that depend on the six variables mentioned and amplitudes that depend on these plus two more that relate δn to δc and δT. Fortunately, for our purposes, the decay rate associated with the temperature relaxation is two to three orders of magnitude faster than the decay rate associated with the diffusion process. For times long compared to the thermal decay time, Eq. 1 can be simplified:

$$\rho \left(\frac{\partial c}{\partial t}\right) \simeq \zeta \left(\frac{\partial \bar{\mu}}{\partial c}\right)_{T,P} \frac{\partial^2 c}{\partial x^2}. \tag{9}$$

This is the usual diffusion equation with:

$$D = \rho^{-1} \zeta \left(\frac{\partial \bar{\mu}}{\partial c}\right)_{T,P}. \tag{10}$$

We obtain the slow decay rate:

$$\tau_2^{-1} = \rho^{-1} \zeta \left(\frac{\partial \bar{\mu}}{\partial c}\right)_{T,P} q_0^2. \tag{11}$$

The chemical potential for water, defined in the Appendix as μ_1, has been measured for both egg yolk lecithin and pure DPPC. According to Eq. A-8 of the Appendix:

$$D = \rho^{-1} \zeta \frac{N_1}{M_1 c} \left(\frac{1}{1 - c}\right)^2 \left(\frac{\partial \mu_1}{\partial N_1}\right)_{T,P,N_2}. \tag{12}$$

Thus the values of D to be reported here together with a measure of $(\partial \mu_1/\partial N_1)$ give an independent measure of the frictional coefficient ζ.

A rough model for ζ can be constructed by assuming the existence of interplanar layers of mobile water within the lamellar phase, as illustrated in Fig. 2. Although we do not expect this to be an accurate representation of the water in equilibrium with the

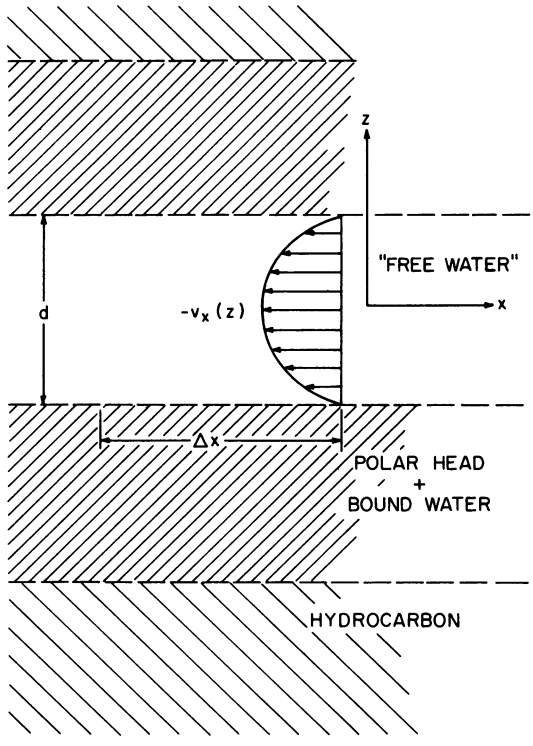

FIGURE 2 Illustration of the model used to obtain the relation between the water diffusion constant and thickness of a free water layer.

lipid, it is a convenient way to model the relaxation phenomena. If the "mobile" water in this layer has the properties of bulk water and if the boundary conditions on either side of the region correspond to zero water velocity, the steady-state Navier-Stokes equation becomes:

$$-\frac{\partial P_w}{\partial x} + \eta \frac{\partial^2 v_x}{\partial z^2} = 0, \tag{13}$$

where $(\partial P_w/\partial x)$ is the effective pressure gradient on the water, η is the shear viscosity of bulk water, and v_x is the local velocity of water in the layer. If $(\partial P_w/\partial x)$ is slowly varying, i.e., $q_0 d \ll 1$, the solution to Eq. 13 with $v_x = 0$ at $z = \pm d/2$ is:

$$v_x(z) = -\frac{1}{2\eta}\frac{\partial P_w}{\partial x}[(d/2)^2 - z^2]. \tag{14}$$

If we define J_x to be the mass flow rate of water per unit layer and per unit length in the y direction, then integrating $v_x(z)$ from $z = -d/2$ to $z = +d/2$ and multiplying by the dentisy of water ρ_w gives

$$-J_x = \frac{\rho_w}{12\eta}\left(\frac{\partial P_w}{\partial x}\right) d^3. \tag{15}$$

In any one layer, the net change in the mass of water Δm_w per unit length along y, in a region of width Δx, during an interval Δt, is given by $-\Delta t[J_x(x + \Delta x) - J_x(x)] = -\Delta t \Delta x(\partial J_x/\partial x)$. The change in mass can be related to the change in concentration: $\Delta m_w/m_w = \Delta c/c(1 - c)$. With Eq. 15, we have:

$$\frac{\partial c}{\partial t} = c(1 - c)\frac{d^2}{12\eta}\frac{\partial^2 P_w}{\partial x^2}. \tag{16}$$

The change in pressure δP_w is related to the change in chemical potential by $\delta P_w = V^{-1}\delta\mu_1$, where V is the molecular volume of water. This can be rewritten as $V^{-1}(\partial\mu_1/\partial c)_{T,P,N_2}\delta c$, so that Eq. 16 becomes:

$$\frac{\partial c}{\partial t} = \left\{\frac{d^2}{12\eta V}(1 - c)c\left[\frac{\partial\mu_1}{\partial c}\right]_{T,P}\right\}\frac{\partial^2 c}{\partial x^2}. \tag{17}$$

For small excursions from the equilibrium concentration, we can identify the diffusion constant as the bracketed term. With Eq. A-7 of the appendix, we obtain the desired result:

$$D/N_1\left(\frac{\partial\mu_1}{\partial N_1}\right)_{T,P,N_2} = \frac{d^2}{12\eta V}. \tag{18}$$

We will see below that our measurements for D and other measurements of $N_1(\partial\mu_1/\partial N_1)_{T,P,N_2}$ obtain values of d that agree very well with independent estimates of the thickness of the free water layer in multilamellar lipid systems.

THE EXPERIMENT

The experimental technique employed for the present measurement is a variation on the forced Rayleigh technique, illustrated schematically in Fig. 3. An intense argon ion laser beam (the pump beam) of wavelength λ_0 = 5,145 Å is split, and the two resulting beams are recombined, intersecting with an angle θ. This produces a sinusoidal interference pattern with wave number:

$$q_0 = \frac{4\pi}{\lambda_0}\sin\frac{\theta}{2}. \tag{19}$$

The pattern is modulated by the Gaussian profile of the laser beam, giving it finite extent. An absorbing sample is placed at this intersection. Where the interference is constructive, the sample absorbs the light and heats up; where it is destructive, the sample has nothing to absorb and can only warm up by heat conduction from the absorbing regions. A sinusoidal temperature distribution with the same wave number is thus created in the sample. Since the local index of refraction depends on temperature, this produces a diffraction grating that will scatter a second, less intense, probe beam if it satisfies the Bragg condition. To understand this point, note that although the interference pattern is periodic along x, it is approximately uniform along the other two directions. The effect is to produce a set of planes that will scatter constructively only if a three-dimensional Bragg condition is satisfied, i.e.:

$$\mathbf{k}_{\text{scatt}} - \mathbf{k}_{\text{incid}} = q_0\hat{x}. \tag{20}$$

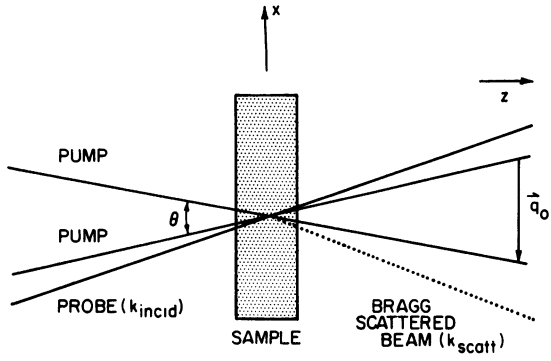

FIGURE 3 Experimental geometry in the vicinity of the sample.

Since the scattering is nearly elastic, this condition corresponds to:

$$(\mathbf{k}_{\text{scatt}})_x = -(\mathbf{k}_{\text{incid}})_x = \pm q_0/2.$$

For a given magnitude of $|\mathbf{k}_{\text{incid}}|$ Bragg scattering will only occur for a specific incident direction.

In addition to a temperature variation, the spatially varying heating pattern will also produce variations in any other variable that couples to the temperature. In the case of DPPC the thickness of the lipid bilayer decreases with increasing temperature throughout much of the phase diagram (14). The effect of this is that in the hotter regions the aliphatic layers become thinner with a slightly increased area per polar head group and water flows from the cooler region to the hotter region to keep the overall smectic repeat distance fixed. In this way initial conditions equivalent to Eqs. 5 and 6 are produced. The heating laser is kept on for a time comparable to the decay time to be measured and then quickly extinguished by a shutter. The intensity of Bragg scattering from the probe beam is observed to decay as δc and δT decay. There are, however, a few subtle points.

Firstly, the relative amplitude of δc_0 and δT_0 (Eqs. 5 and 6) is dependent upon the length of time that the heating pulse is on as well as upon a combination of the dissipative parameters and thermodynamic derivatives of the hydrodynamic theory (the Soret coefficient). There is no thermodynamic restriction on the magnitude or the sign of this coefficient, so that although we have just described a situation where water flows from a cool to a warm region, there is no reason the water cannot flow the other way.

Secondly, the hydrodynamic results described previously tacitly assumed that there were no other variables, such as defects in the smectic layers or intramolecular coordinates, that had relaxation rates comparable to the hydrodynamic relaxation rates described above. In general this is consistent with our measured results; however, there are some exceptions.

Thirdly, in addition to the sinusoidal variation in the heating pattern, there is a slower variation that corresponds to the width of the laser beams. Assuming a Gaussian beam of width a, a realistic intensity profile would be

$$I(x, y) = I_0(1 - \cos[q_0 x + \psi])\, e^{-(x^2+y^2)/a^2}, \tag{21}$$

where ψ gives the locations of the maxima and minima of the grating. Random defects or imperfections can cause scattering due to the background term (independent of q_0) into the same directions as the Bragg term. The characteristic times for the decays of this scattering are $4\chi/a^2$ and $4D/a^2$ for the temperature and concentration contributions, respectively. Here, χ is

the thermal diffusivity and D is the diffusion constant. This can be a problem if $4\chi/a^2 \simeq Dq_0^2$, since there would be an unwanted decay with approximately the same decay time as one we are trying to observe. This is indeed the case with the phospholipid-water samples we use.

A variation on forced Rayleigh scattering circumvents this problem. Note that the phase of the electric field of the Bragg scattered light is a linear function of the phase ψ of the grating, while the light scattered from the background heating is independent of the grating phase. We can retain the phase information in the scattered light if we use optical heterodyne detection, that is, if we mix the scattered light with a reference in a nonlinear device such as a photomultiplier tube (PMT). The photon count rate $\dot{n}$ is approximately

$$\dot{n} = g|E_r|^2 + 2g\sigma_s|E_r||E_s|\cos(\phi_s + \psi) + 2g\sigma_B|E_r||E_B|\cos\phi_B, \qquad (22)$$

under the assumption that $|E_r| \gg |E_s|, |E_B|$, where E_r, E_B, and E_s are the complex, slowly varying reference, background, and Bragg scattered electric fields, respectively; g is a constant dependent upon the geometry and PMT quantum efficiency (15). σ_s and σ_B are numerical factors with $|\sigma_s|, |\sigma_B| \leq 1$ that arise from the fact that the photon count rate is an integral over the area of the photocathode: neither the amplitudes nor phases of the optical fields are actually constant over this area and the mixing beams may not exactly overlap. The phases ϕ_B and ϕ_s are defined relative to the reference beam. By alternately changing ψ between $-\phi_s$ and $\pi - \phi_s$ while synchronously adding and subtracting the photocounts from the memory of the data collection electronics, we discriminate against non-Bragg scattering. Thus after $2N_s$ heating pulses with ψ alternating by π, the term that couples linearly to the interference grating will grow linearly with N_s, while the scattered light that does not arise from the Bragg effect averages to zero except for shot noise effects. Aside from the shot noise, which will be discussed below, we are left with the desired decay.

A detailed schematic illustration of the experimental setup is shown in Fig. 4. The pump beam is from an argon ion laser of several hundred milliwatts operating at 5,145 Å; the probe beam is from a 2 mW helium-neon laser (6,328 Å). Both beams are polarized normal to the scattering plane. The pump beam is turned on and off with a mechanical chopper and

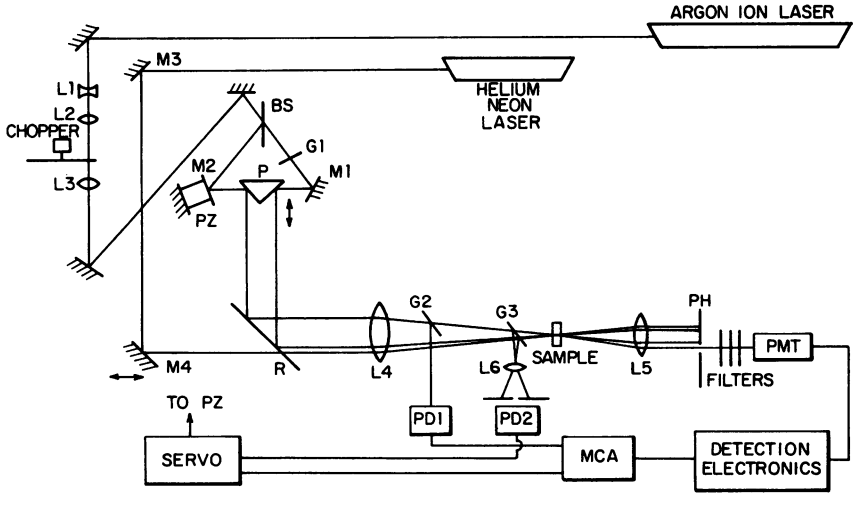

FIGURE 4 Schematic illustration of the experiment, showing details of the optics and block diagrams of the electronics. Further details are contained in the text.

the experiment is repeated N_s times with the resultant signals alternatively added and subtracted to the memory. The on-time is adjusted to be one or two times the decay time under study, as this obtains the maximum magnitude for the intensity of the sinusoidal grating relative to the background. The off-time is at least seven times longer than the on-time to allow the temperature or concentration grating amplitude to decay to a value comparable to that produced by statistical fluctuations. The pump beam is split with a 50-50 beam-splitter (BS). The path length of one of the split beams can be varied by a piezoelectronic device (PZ) for the purpose of fixing ψ at either $-\phi_s$ or $\pi - \phi_s$. The two pump beams and the probe beam are made parallel and coplanar, and are focused with a long focal length lens L4 into the sample, where the beam diameters are about 1 mm. By varying the separation of the pump beams we can change q_0 without moving the point of intersection and without changing the width a. The probe beam is moved laterally by translation of M_4 until it goes into the sample at the Bragg angle. Elastic scattering due to static defects of micron size inside the sample produces the reference field E_r.

The collection optics consist of lens L5 and pinhole (PH) located one focal length behind L5; this arrangement selects out light traveling in a particular direction. Behind the pinhole are a Wratten filter to block the pump beam, neutral density filters, a polarization analyzer, and a 6,328-Å spike filter. The filters show no sign of fluorescence. Only at full power of the argon laser and with the pinhole removed does the Wratten and spike filter combination show signs of transmission. The photomultiplier tube is an ITT FW130 with a S-20 photocathode (ITT Electro-Optical Products Div., Roanoke, Va.). The dark count is 400 counts/s, much smaller than the shot noise of the reference beam. There are two glass slides between L4 and the sample to reflect small fractions of the pump beams to electro-optical devices PD1 and PD2 for timing and the control of the grating phase.

With this set-up, wavelengths $2\pi/q_0$ from 20 to 150 μm are possible. Note also that because of translational invariance in the x direction, the grating wavelength is the same inside and outside of the sample, and no index of refraction correction is necessary.

The photopulses from the PMT are amplified, passed through a discriminator, and counted in a 1,000-channel multichannel analyzer (MCA). The MCA is an instrument that gives a histogram of the arrival times of the photopulses relative to the turn-off time of the heating laser beam. It has been suitably modified to add and subtract on alternate sweeps to effect the averaging described earlier. The channel width T_c, i.e., the time resolution of the MCA, is adjusted so that the full time range (1,000 T_c) is three or four times the decay time τ.

Under our experimental conditions, the primary noise source is shot noise from the reference beam. If we assume Poisson statistics for the photopulses, the noise in a single channel after N_s sweeps is:

$$N = (gN_sT_c)^{1/2} \mid E_r \mid . \tag{23}$$

According to Eq. 21, the average signal in that channel is:

$$S = 2g\sigma_s \mid E_r \mid\mid E_s \mid N_sT_c, \tag{24}$$

where we assume the phase between the reference and signal has been optimized, and the signal-to-noise ratio (SNR) is:

$$\text{SNR} = 2(gN_sT_c)^{1/2}\sigma_s \mid E_s \mid . \tag{25}$$

Note that the add-subtract technique does not enhance the SNR, in that the shot noise from the cancelled constant background $\mid E_r \mid^2$ is still present. However, the time-dependent signal due to E_B is eliminated by this technique and this has previously been the principal limiting factor in detecting a small diffusion signal in the presence of a larger thermal effect. Since

the SNR is proportional to $T_c^{1/2}$, we can improve the SNR at the expense of time resolution if we add the contents of several adjacent channels to form what will be effectively a single channel. Indeed, in the data analysis we would often add the counts from four channels to double the SNR and reduce the resolution from T_c to $4T_c$.

SAMPLE PREPARATION

The homeotropic multilamellar phospholipid-water samples are made by a technique described by Powers et al. (7, 16). There are two significant departures from this procedure: first, the phospholipid is purified by column chromatography before use. Second, β-carotene is added to the samples to give the otherwise colorless DPPC-water samples optical absorption at the pump laser wavelength.

The phospholipid we use is L-α-dipalmitoyl phosphatidylcholine (DPPC) from Calbiochem (grade A, San Diego, Calif.) and Sigma Chemical Co. (St. Louis, Mo.). We have run the forced Rayleigh experiment on samples made with purified and unpurified DPPC and have found no difference in results. However, as we shall describe, the purified DPPC is found to be easier to use, and all results reported here have been obtained with the purified DPPC. The purification is done by eluting DPPC from a silica gel, (Bio Sil A, 200–400 mesh, Bio-Rad Laboratories, Richmond, Calif.) -chloroform slurry with methanol. The purified DPPC is stored dry under nitrogen in the dark in a freezer. We monitor its purity by thin-layer chromatography before use.

The dye, β-carotene, was chosen with several properties in mind. It has a high absorption cross-section at the pump laser wavelength, so that only a small contribution is needed to give the absorption necessary for the forced Rayleigh scattering experiment (the attenuation coefficient is about 1 cm^{-1} at the pump wavelength). Because β-carotene is lipophilic and its length is shorter than the bilayer hydrocarbon region thickness, it is reasonable to expect it to reside solely in the hydrocarbon layer and to have a minimal perturbation on the water diffusion.

One problem with the β-carotene, however, is its tendency to bleach, i.e., to lose its absorption at visible wavelengths, during the sample preparation process or the experiment. The bleaching process may be attributed to a free radical reaction (17), with the original free radicals being either peroxides of β-carotene formed by photo-oxidation, or impurities introduced in either the synthesis or subsequent handling of either the β-carotene or DPPC. For this reason, both are purified and kept under nitrogen with as little exposure to light as possible. We are able to make aligned samples that do not bleach containing comparable molar concentrations of β-carotene and butylated hydroxyl toluene (BHT), a free radical trap; but this is an undesirable way to do the experiment because it adds an unnecessary impurity.

The β-carotene, obtained from Sigma Chemical (grade A), is purified by repeated precipitation out of a CS_2-β carotene solution (18, 19). Precipitation follows on addition of methanol, approximately in the volume ratio of methanol: CS_2 of 4:1. The final precipitation is done with nitrogen-distilled petroleum ether by making a saturated solution just below the petroleum ether boiling point and cooling the solution slowly to 0°C. The crystals are about 100 μm in size and show a metallic shimmer. They are stored in a light-tight vial under nitrogen at 0°C. One indication of the purity is that, unlike the unpurified material, the recrystallized material is odorless. Also, visible and near-ultraviolet absorption spectra of the purified material in solution are identical to published spectra of β-carotene solutions (20). Finally, thin layer chromatography shows only one component.

As the first step of sample preparation, the DPPC and β-carotene are mixed by freeze-drying them from a solution of nitrogen-distilled benzene. Enough β-carotene is added to DPPC to make two or three samples (about 5 mg each) that are 0.005 M in β-carotene. This mixture is always used immediately after taking it from vacuum.

The sample geometry and alignment techniques are identical to those described by Powers and Pershan (7) and the reader is referred there for the details. Briefly, however, a small amount of water, less than 10% by weight, is added to the mixture and it is placed between two suitably treated glass slides that are separated by a 0.005-inch Teflon spacer with a 1/4-inch diameter hole. The spacer completely surrounds the mixture and, except for a removable section, the glass plus spacer forms a sealed disk-shaped cavity. The entire assembly procedure is carried out under a dry nitrogen atmosphere and when necessary can be stored under nitrogen and in the dark for up to several days without noticeable degradation. Oriented, or aligned, multilammellar samples result from the annealing procedure first described by Powers and Clark (16). In our samples annealing occurred at temperatures that varied between 120°C and 150°C, depending on the precise amount of water added to the mixture.

After alignment is achieved, additional water can be added to the sample as described by Powers and Pershan (7). A part of the Teflon spacer surrounding the DPPC-mixture is removed and the sample is immersed in deoxygenated distilled water, usually at 85°C, for times that vary from a few minutes to 5 h depending on the amount of water to be added. For samples to be studied at high temperatures, water addition was done just below 100°C. Aligned samples with added water were kept at 80°C or higher for 10 h to equilibrate. Sample alignment and homogeneity were monitored optically as in Powers and Pershan (7). It does not appear as though the β-carotene affects either the sample alignment or homogeneity in any way. The sample has a uniform yellow hue and there is no evidence of clustering effects that would indicate phase separation. On the other hand, when a sample, with or without β-carotene, is placed inside the forced Rayleigh scattering apparatus, one can visibly observe depolarized light scattering within a cone of about 10° surrounding the laser beam. Although we have not made a systematic study of this effect, microscopic observation of the alignment process in other DPPC samples indicates occasional defects of micron size, separated by well-aligned regions of the order of 100 ~ 500 μm that could be responsible for it. The wave vector dependence of the observed relaxation rates would seem to preclude the possibility that these occasional defects have significant influence on the results. In any event, this static scattering is a convenient way to obtain the reference field required for heterodyne detection.

During the measurement the sample is maintained in a vertical position inside an oven whose temperature can be set to a precision of ±0.1°C and remains stable to ±0.01°C over the duration of the experiment. For much of the phase diagram the smectic repeat distance of DPPC decreases with increasing temperature. Since the samples we use are of fixed thickness, the effect of raising the temperature would be to induce an anisotropic stress tending to oppose the decrease. There is a well-documented instability in smectic liquid crystals subjected to this type of stress, and if alignment is to be maintained, it is important that samples always be measured as a function of decreasing temperature (21–23).

After a series of measurements at different temperatures on a sample, the water content is determined by a gravimetric method. The lipid is removed from between the glass slides and weighed. It is then heated to approximately 100°C for 12 h under a 10-μm vacuum, after which it is permitted to cool *in vacuo* for 6–8 h. The vacuum is relieved by blowing dry nitrogen into the vacuum dessicator, and the sample is reweighed within 30 s of its removal from the dessicator. We assume the weight difference is due to the loss of water. The estimated precision in weight fraction of water is 1%. For samples with less than 20% water by weight, where the gel transition temperature is a strong function of water concentration, the water concentrations determined by this method agree with those deduced by visually observing the gel transition in our samples (7).

RESULTS AND DATA ANALYSIS

The recorded data consist of a set of numbers $\{y(x)\}$ corresponding to the number of counts stored in the set of channels $\{x\}$, $x = 1, \ldots, 1{,}000$. As mentioned pre-

viously, it is sometimes convenient to combine data in adjacent channels such that the effective number of channels in the fitting procedure is $N_{\text{fit}} = 500$ or 250. The data were fit to theoretical curves that had one of the following forms:

$$y^{(2)} = a_1 e^{-a_2 x}, \tag{26a}$$

$$y^{(3)} = a_1 e^{-a_2 x} + a_3, \tag{26b}$$

$$y^{(4)} = a_1 e^{-a_2 x} + a_3 e^{-a_4 x}, \tag{26c}$$

$$y^{(5)} = a_1 e^{-a_2 x} + a_3 e^{-a_4 x} + a_5, \tag{26d}$$

where $\{a_i\}, i = 1 \ldots m$, are the fitting parameters.

Under the conditions of our experiments only exponential decays are expected and Eq. 26*d* is adequate to fit all of our results. The other forms are used only when data do not warrant a five-parameter fit. For example, if the slower of the two decays is longer than the sweep time of the MCA, 1,000 T_c, the slower decay appears as a constant and Eq. 26*b* can be used in place of 26*d*. In many instances more than one form was tried. The fitting routine does a nonlinear least-square fit, i.e., minimizes the quantity:

$$\chi^2(\{a_i\}) = \frac{1}{gT_c N_s |E_r|^2 (N_{\text{fit}} - m)} \sum_{x=1}^{N_{\text{fit}}} [y_{\text{data}}(x) - y_{\text{fit}}^{(m)}(x)]^2, \tag{27}$$

with one of these functional forms (24). We find that the final values of $\{a_i\}$ do not depend strongly (less than one part in 10^4) on the initial guess—guesses known to be wrong by two orders of magnitude, for one or more of the $\{a_i\}$'s lead to the same $\{a_i\}$ as those resulting from more reasonable initial values. We estimate the uncertainty in any fitting parameter by varying that parameter while simultaneously allowing the fitting routine to adjust the others in order to keep χ^2 at a local minimum. The uncertainty in $\{a_i\}$ is specified by those deviations that cause χ^2 to increase by unity.

The difference $\epsilon(x)$ between the fit and the data is visually examined to determine if the fit is good. Furthermore, the autocorrelation function of the error,

$$R(x) = \sqrt{N_{\text{fit}}} \sum_{x'=1}^{\left[\frac{N_{\text{fit}}}{2}\right]} \epsilon(x')\epsilon(x' + x) \Big/ \sum_{x'=1}^{\left[\frac{N_{\text{fit}}}{2}\right]} \epsilon^2(x'), \tag{28}$$

with

$$\epsilon(x) = y_{\text{data}}(x) - y_{\text{fit}}^{(m)}(x) \tag{29}$$

is plotted to see if there are any systematic errors and to confirm that the form of the decay is adequately represented by Eq. 26. If there are no systematic errors, $R(x)$ should equal $\sqrt{N_{\text{fit}}}$ at $x = 0$ and fluctuate randomly with a root mean square value of unity for $x \neq 0$. Fig. 5 shows typical fits and autocorrelations. In the examples

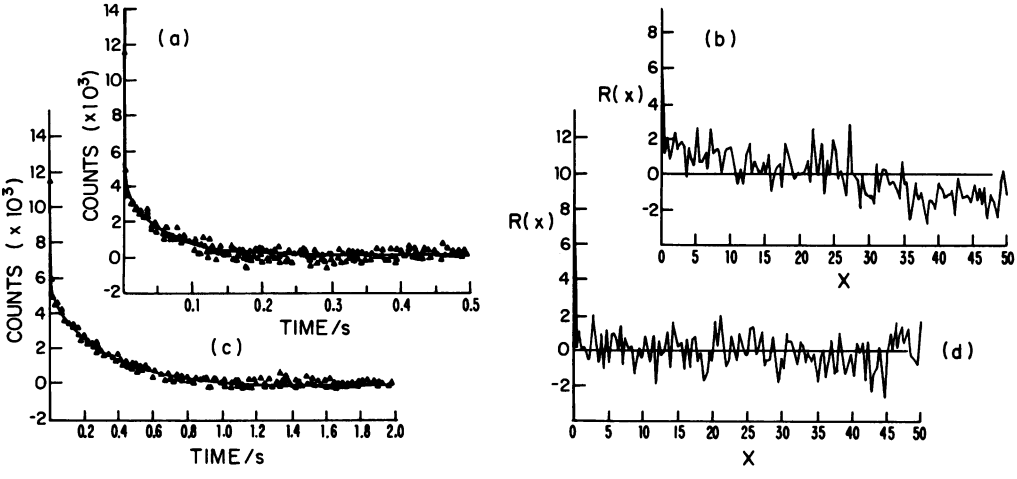

FIGURE 5 Typical decays, fits, and error correlations. These show the decay due to water diffusion for (*a*) $q_o = 938\ \text{cm}^{-1}$, $T = 85°\text{C}$, and $c_w = 17\%$ and (*c*) $q_o = 524\ \text{cm}^{-1}$, $T = 65°\text{C}$, and $c_w = 20\%$. The first two points in each are fast decays due to thermal diffusivity. The χ^2 of the fits are 0.96 and 1.02, respectively. The corresponding error correlations are shown in *b* and *d*. It is apparent from these that *c* has a better fit, though this is not obvious from ϵ or χ^2.

given, χ^2 and $\epsilon(x)$ are similar, but $R(x)$ shows that one of them has a small systematic error when fitted to the sum of two exponentials and a constant. In principle, the fitting parameters could be adjusted to remove this systematic error. In practice, the effort involved in calculation of $R(x)$ is much more than the effort to optimize the fit for minimum χ^2. Furthermore, the changes in fitting parameters that eliminate the systematic deviations are less than the uncertainty estimated from the χ^2 fit. We did not attempt to reduce the uncertainty in fitting parameters through use of $R(x)$. Although this is possible, the data do not warrant the extra effort.

We have measured these modes at various water concentrations and temperatures, all with the wave vector in the plane of the smectic layers. To obtain a diffusion constant or thermal diffusivity at a particular water concentration and temperature, we measure the decay rates for three to eight wave numbers. We plot the rates vs. wave number on log-log paper and find the best fit assuming a priori a square law dependence. A typical fit of this type is shown in Fig. 6. Since the fastest decay rates accurately measurable by an apparatus are approximately $3 \times 10^3\ \text{s}^{-1}$, the thermal decay rate corresponding to $q^0 = 2.5 \times 10^3\ \text{cm}^{-1}$ is not reported.

As we have said, the forced Rayleigh data generally show two exponential decays with characteristic decay times that differ by about a factor of 100. The decay rate of the faster one has a q_0^2 dependence for values of the wave number larger than an inverse sample thickness. It has a diffusivity consistent with the thermal diffusivity of organic fluids and we identify it as the thermal diffusive mode. For smaller values of q_0 the decay rate is independent of wave vector due to a "short-circuiting" of the heat flow through the glass plates. The slower decay rate also has a q_0^2 dependence, but with no apparent leveling off at an inverse sample thickness. According to the

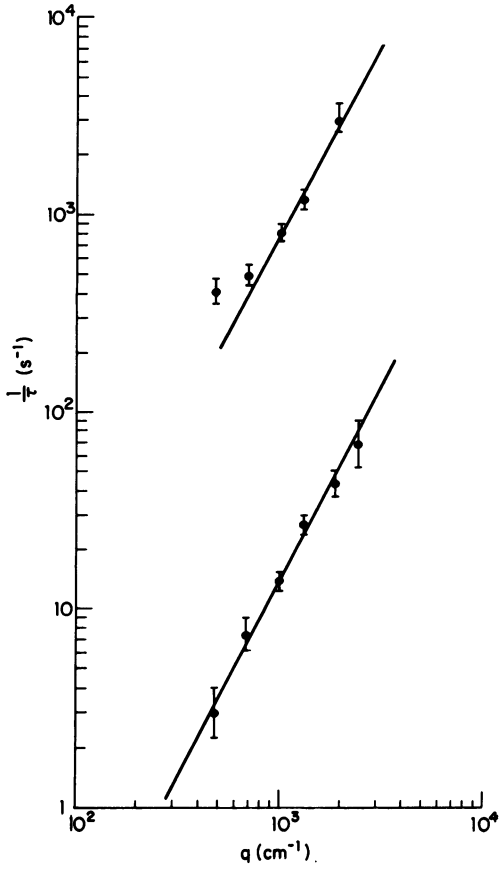

FIGURE 6

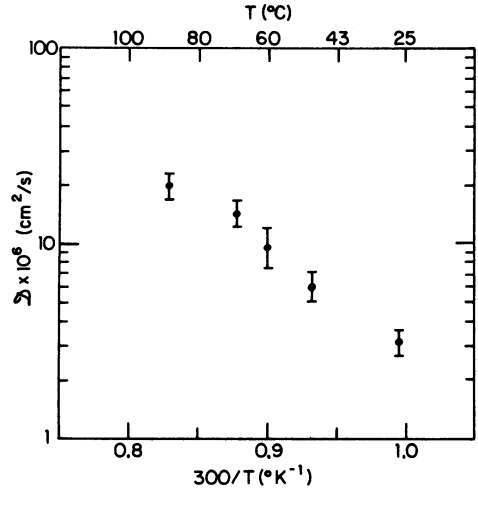

FIGURE 7

FIGURE 6 Plots of the decay rates versus q_o at T = 70°C and c_w = 24%. The upper set gives the dispersion relation for the thermal diffusivity; it saturates at a wave number corresponding to the sample thickness (125 μm). The lower set is for the water diffusion, and does not saturate.
FIGURE 7 The temperature dependence of the diffusion constant at c_w = 21% plotted to show an Arrhenius behavior with E_a = 0.32 eV.

hydrodynamic theory (8), the only possibilities for decay rates with this property are either a diffusive mode in which the relative water-to-lipid concentrations relax (predominantly a water relaxation) or diffusion of some other species. Both the relaxation rate and signal amplitude are so much larger than any reasonable estimate of what might be expected from the only other chemical species (β-carotene) in our samples that we discount that possibility. The slower relaxation rate is then identified as the hydrodynamic mode discussed by Brochard and de Gennes (8), i.e., the "water diffusion" mode.

The results for the thermal diffusivity are presented in Table I. We see that the measured values change by less than a factor of 2.2 over the wide range of water concentrations and temperatures used. This is consistent with the relative insensitivity

TABLE I

THERMAL DIFFUSIVITIES IN DPPC-WATER

T	Weight % water					
	4	17	20	21	24	35
$C°$			$\chi \times 10^3, cm^2/s$			
85	0.7	1.0	1.1 (5%)			
80						1.0
75		1.1 (20%)				
70				0.95	0.75	
65	0.5	0.6				
50				0.95		

Unless otherwise indicated, errors are 10%. Each column has measurements from only one sample.

of thermal diffusivities to the details of the system. The slower relaxation rate, corresponding to the diffusion constant, shows considerable variation with temperature in the region of the phase diagram where measurement was possible. We thus studied this relaxation more extensively than the thermal decay, and there is more data on the diffusion constant presented in Table II than in Table I.

It is useful to plot the diffusion constant as a function of temperature at constant water concentration and as a function of water concentration at constant temperature. These are done for $c_w = 21\%$ and $T = 70°C$ in Figs. 7 and 8.

In the constant concentration plot, the diffusion constant decreases with decreasing temperatures. This trend is seen at the other water concentrations. Though the data

TABLE II

DIFFUSION CONSTANTS IN DPPC-WATER

T	Weight % water								
	8	10	15	17	20	21	24	24	35
°C					$D \times 10^6, cm^2/s$				
100	1.5 (50%)	2.7							
95									
90		2.3 (30%)				20			
85				15 (40%)	19				
80		0.9			16 (40%)				
75				14					
70		0.8 (40%)	16	9.7	12	14.5	13	12	12
65				9.2	12				
60			11 (50%)			9.6	12 (10%)	13	
55				8.0					
50						6.1			
45							7.7		
30						3.2			
20							3.9		

Unless otherwise indicated, errors are 20%. Each column has measurements from only one sample.

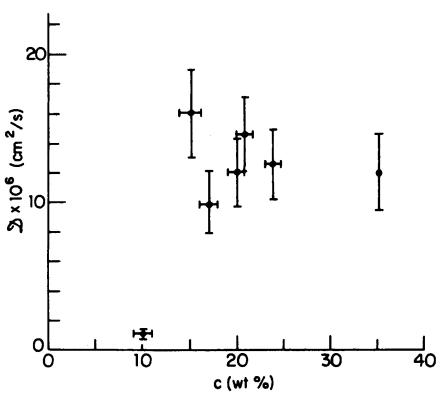

FIGURE 8

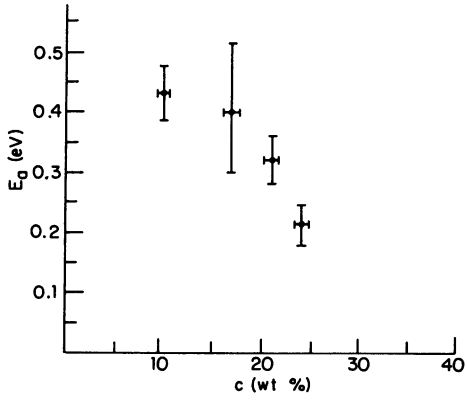

FIGURE 9

FIGURE 8 The concentration dependence of the diffusion constant of water at $T = 70°C$.
FIGURE 9 The activation energy for water diffusion as a function of water concentration. For comparison, the activation energy for the self-diffusion of water is 0.17 eV.

are not precise enough nor the temperature range large enough to completely justify it, we can fit the diffusion constant reasonably well to an Arrhenius relation: $D = D_0 e^{-E_a/k_B T}$, where E_a is the activation energy for the diffusion process. The activation energy as a function of water concentration is plotted in Fig. 9, where we see a systematic decrease with increasing water concentrations. By way of comparison, the activation energies for both the shear viscosity and the self-diffusion coefficient of bulk water are 0.17 eV.

Elworthy measured $(\partial\mu_1/\partial N_1)_{T,P,N_2}$ (see Eq. A-8 of the Appendix) for DPPC and obtained nearly identical results at 25°C and 40°C (25, 26). It thus seems reasonable to assign the temperature dependence that we observe for D to the frictional coefficient ζ (see Eq. 10). We can thus interpret the activation energy that we now associate with ζ as the average energy barrier a water molecule must overcome to move from one site to another. This will be larger than the value for bulk water either because of direct interactions between water and polar head groups or because the water structure surrounding the phospholipid molecules is more rigid than the structure in bulk. For either reason one expects the effects to become less important at higher water concentrations and the activation energy to decrease. This is the behavior depicted in Fig. 9.

The concentration dependence of D is shown in Fig. 8 for $T = 70°C$. The diffusion constant is small ($\sim 10^{-6}$ cm^2/s) at 10% water and increases by an order of magnitude between 10 and 15%. Between 15 and 24%, it remains at about the same value and the data discussed below support the contension that it is the same at 35% If we assume that Elworthy's values for $(\partial\mu_1/\partial N_1)_{T,P,N_2}$ at 25°C and 40°C are also applicable at 70°C, we can use either Eq. 10 to obtain values for ζ, or Eq. 18 to obtain values for the effective thickness of the "free water layer":

$$d_{eff} = \{12\eta VD\}^{1/2}[N_1(\partial\mu_1/\partial N_1)_{T,P,N_2}]^{-1/2} \tag{30}$$

Fig. 10 is a plot of $D[N_1(\partial\mu_1/\partial N_1)_{T,P,N_2}]^{-1}$ versus water concentration using both Elworthy's data for DPPC and values extrapolated to lower water concentrations from similar results obtained by LeNeveu et al. for egg yolk lecithin at higher water concentrations (27). One might guess that the chemical potential for water in egg yolk lecithin would not be significantly different from that of DPPC at the temperature and water concentrations of our experiments. For example, if the data presented by LeNeveu et al. (27) is extrapolated to low water, one expects that $N_1(\partial\mu_1/\partial N_1)_{T,P,N_2}$ will vary by nearly three orders of magnitude as N_1 varies from about 2 to 30 water molecules per lipid. On the other hand, the largest differences between Elworthy's and LeNeveu's results for $N_1(\partial\mu_1/\partial N_1)_{T,P,N_2}$ are no more than a factor of five or six at comparable water concentrations. Fig. 10 illustrates the values of $D/N_1(\partial\mu_1/\partial N_1)_{T,P,N_2}$ obtained from these two measurements and our results for D. According to Eq. 30, $d_{(\text{eff})}$ varies as the square root of this ratio, so that the discrepancy of a factor of six in $N_1(\partial\mu_1/\partial N_1)_{T,P,N_2}$ produce a much smaller variation in $d_{(\text{eff})}$. This can be compared with an estimate that Small (5) made of the thickness of the free water zone based on X-ray diffraction data and the arbitrary assumption that the polar head groups are maximally extended a distance of 8 Å into the total water thickness. His results are also shown in Fig. 11, and one can see excellent agreement with the results of our estimate using the LeNeveu data and diffusion measurements. Actually, the theory that leads to Eq. 30 is too crude to make any distinction between the results based on Elworthy's data in comparison with LeNeveu's. The quality of the agreement,

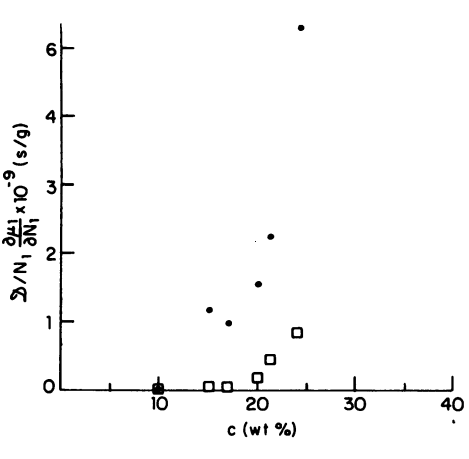

FIGURE 10

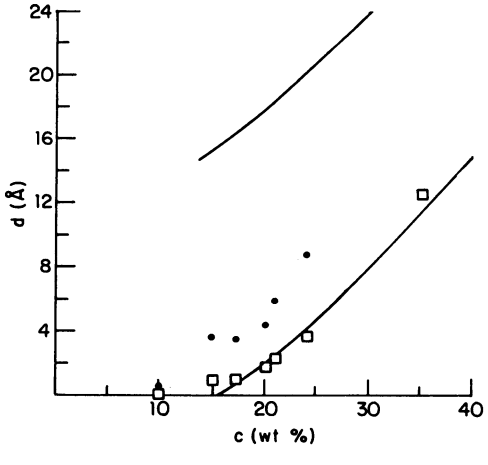

FIGURE 11

FIGURE 10 $D(N_1\partial\mu_1/\partial N_1)^{-1}$ at T = 70°C as a function of water concentration. This quantity is related to the dissipative parameter ζ by Eqs. 10 and A-8, and to model parameters by Eq. 18. The points marked • and □ are obtained using Elworthy's (25, 26) and LeNeveu et al.'s (27) results, respectively, for the chemical potential.

FIGURE 11 d_{eff} versus c_w at T = 70°C, assuming the viscosity of bulk water at this temperature (0.40 cP). The symbols are the same as in Fig. 10. The upper curve gives Small's estimate of the total water thickness, while the lower one gives his estimate of the free water zone thickness (5).

however, strongly supports Small's contention concerning the effective thickness of the free water layer. Note also that the water concentration at which $d_{(eff)}$ approaches zero corresponds to about five water molecules per polar head group. This coincides with other estimates of the amount of water required to complete an intermediate hydration shell of DPPC (5).

For most q vectors the observations at 35% water indicate three exponential decays rather than the two predicted from the hydrodynamic theory. The fastest of these behaves similarly to the thermal decay in lower water samples and will not be discussed further. Although the origin of the extra slow decay cannot be explained in the context of a rigorous hydrodynamic theory, it would not be surprising to observe interference effects between an unidentified nonhydrodynamic mode and the existing hydrodynamic mode. A conventional, although somewhat speculative, interpretation of the data is obtained on fitting the wave vector dependence to the theoretical form:

$$(1/\tau)_{\pm} = \frac{1}{2}(\tau_0^{-1} + Dq^2) \pm \frac{1}{2}[(\tau_0^{-1} - Dq^2)^2 + 4\zeta^2 q^2]^{1/2}, \tag{31}$$

that can be shown to result from coupling between a relaxation process with $(1/\tau) \simeq Dq^2$ and one independent of q_0, $1/\tau = 1/\tau_0$. It follows that if the coupling parameter $\zeta = 0$, Eq. 31 reduces to these two forms. Although conjectures on the physical origin of this extra decay mode and the coupling parameter ζ are possible, in the absence of more information these would be very speculative. If, for example, there were localized defects in the DPPC bilayers that could change either size, shape, or orientation in response to local stresses, their relaxation would couple to the water relaxation in this way. Fig. 12 indicates a number of experimental points together with the "best" theoretical fit obtained from Eq. 31. Although it was not possible to extract both τ_+ and τ_- from all measurements, we believe the consistency between *all* recorded data and this model makes the interpretation credible. The facts that the characteristic length estimated from either $\tau_0\zeta$ or D/ζ is of the order of 10 μm and that the characteristic time is 13 s^{-1} suggest the extra relaxation process is the result of a structural deformation. In spite of the rather speculative nature of this fit, if the value for D obtained from this fit is used to obtain a value for $d_{(eff)}$, the result agrees well with Small's estimate of the thickness of the free water layer at 35% water. The data point for 35% water in Table II and Fig. 8 is the result of this interpretation.

The relative amplitudes of the two modes (water decay amplitude/thermal decay amplitude) is about 0.9 for 24% water, 0.4 for 20% water, 0.3 for 17% water, -0.5 for 10% water, and -0.3 for 8% water. There are large errors associated with these; however, the sign is reproducible with samples of the same water content and does not change with either wave vector or temperature within a sample. When the sign is positive, it is consistent with the water layer swelling at the hot regions. We could not detect a temperature dependence of this ratio.

In the 24% water sample, we observe a hydrodynamic decay slower than that of thermal conductivity or water diffusion. It has a diffusion constant of 6.4×10^{-7}

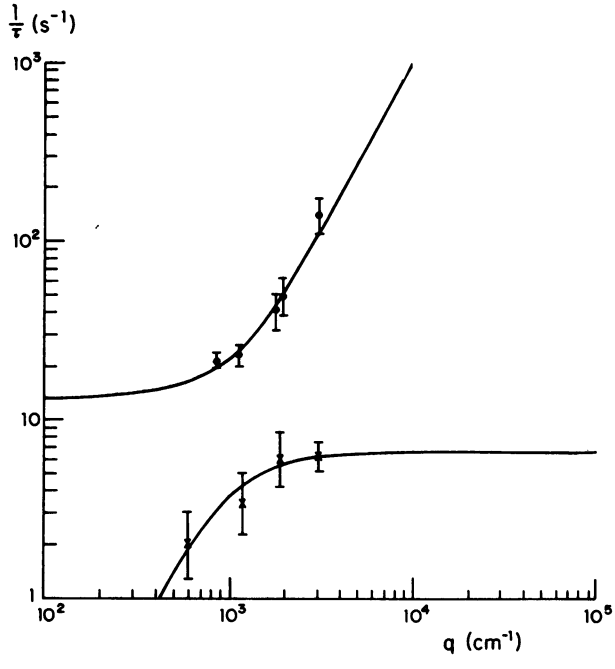

FIGURE 12 Fit of water diffusion data obtained at $T = 70°C$ and $c_w = 35\%$ to Eq. 31. The fitting parameters are $D = 1.2 \times 10^{-5}$ cm^2/s, $\tau_0^{-1} = 13$ s^{-1}, and $\zeta = 9.0 \times 10^{-3}$ cm/s.

cm^2/s at 70°C and 1.0×10^{-7} cm^2/s at 22°C. We expect that this may be the diffusion coefficient of β-carotene inside the lipid. For example, olive oil has fatty acid lengths comparable to those of DPPC. The viscosity of olive oil is known for different temperatures (29), and the ratio of these two diffusion coefficients is equal to the ratio of the viscosity of olive oil at these same temperatures. This is the result expected from the Stokes-Einstein formula for diffusion of an impurity within the hydrocarbon part of the lipid bilayer. Using this viscosity, we find that Stokes radius of the diffuser to be 2.6 Å.

DISCUSSION

Independent measurements of water diffusion within lamellar phases of egg yolk lecithin have been made by Lange and Gary Bobo (30), for mixtures of egg yolk lecithin and cholesterol by Inglefield et al. (31), and for dimyristoyl phosphatidylcholine by Lindblom (32) as a function of water concentration. In all three cases the diffusion coefficient increases with increasing water concentration up to about 24% water. For example, Inglefield et al. (31) report room temperature values of D_{H_2O} that vary from about 2.3×10^{-6} cm^2/s at 15% water to a maximum of 4.5×10^{-6} cm^2/s at 25% water in a "lecithin-cholesterol" mixture. For slightly higher water concentrations, the diffusion coefficient decreases by about a factor of four and remains at this lower value for further increases in the amount of water. Lange and Gary Bobo interpreted this

phenomenon in terms of some type of structural transformation. Electron spin resonance studies on egg yolk-lecithin-water mixtures indicate anomalies at approximately the same water concentration (33). Furthermore, other studies have demonstrated anomalies at 20 wt% water (for dipalmitoyl phosphatidylcholine) (7), and thus it would be reasonable to expect the values of D reported here to display a precipitous drop at this same water concentration. No such effect was observed.

Below 20 wt % water our results for the water diffusion coefficient are reasonably close to the values obtained by Lange and Gary Bobo (30) and Inglefield et al. (31) at comparable temperatures, suggesting that water diffusion in egg yolk lecithin and DPPC should be essentially the same. Thus it is difficult to rationalize the different behavior of D at higher water concentrations. The explanation that appears most likely to us is that the nuclear magnetic resonance techniques employed by Inglefield et al. (31) and by Lindblom (32) and the trace diffusion technique of Lange and Gary Bobo (30) both measure the self-diffusion coefficients of individual molecules rather than the hydrodynamic coefficient associated with the relaxation of a macroscopic water concentration inhomogeneity. For very low water content these two would have to be essentially the same, in agreement with the measured values. For higher water, this need not be the case, since it is not obvious that an individual molecule, moving by a thermally driven random walk process, would cause any elastic distortion of the lipid lamellae. Since this is the driving force for the concentration relaxation, the two types of diffusion constants would differ.

On the other hand, it is difficult to understand why the diffusion constant for an individual molecule should decrease with increasing water. Gary Bobo's interpretation of a phase transition of some sort at about 20% water is reasonable in view of the anomalies seen in other experiments. Nevertheless, we are at a loss to find a plausible physical argument to explain a decrease in D starting at 20% water. We believe the trends displayed by our results are much more plausible.

To summarize, the principal contributions of this paper are: (*a*) A new experimental technique based on forced Rayleigh scattering is reported. The significant innovation is to utilize the phase information in the scattered light to enhance the ability to separate weak signals from strong background scattering. (*b*) The application of this technique to measure the thermal and concentration relaxations in lamellar DPPC-water samples at varying temperatures and water concentrations is described.

The thermal diffusivity is about 8×10^{-4} cm^2/s and does not change much in the portion of the DPPC-water phase diagram we studied. This value is consistent with that of an organic fluid.

The diffusion constant ranged from 0.8 to 20×10^{-6} cm^2/s. At 70°C, it is approximately constant above 15% water, and decreases by over an order of magnitude at lower water concentrations. These results together with published data on the chemical potential of water in DPPC obtain a measure of the effective thickness of a free water layer in excellent agreement with estimates of others. The diffusion constant shows an Arrhenius behavior with activation energies plausible both in magnitude and as a func-

tion of water concentration. The energy at low water is about twice as large as that associated with the self-diffusion of water, and monotonically decreases toward this self-diffusion value at higher water concentration. Since estimates of the amount of free water are often based on measurements of the "ice peak" as observed in calorimetry (34), it is particularly significant that our estimate of the free water thickness is obtained from measurements at 70°C.

We would like to express our appreciation to Dr. E. A. Dawidowicz of the Harvard Medical School for instruction in methods of purifying our lipid materials. We also would like to express our appreciation to Dr. Sanford Asher for help in other chemical aspects of this project. Dr. Linda Powers was of invaluable help in providing instructions on the techniques of making aligned samples.

This work was supported in part by the Joint Services Electronics Program (U. S. Army, Navy, and Air Force) under contract N00014-75-c-0648 and by the National Science Foundation under grants DMR-76-0111 and DMR-76-22452.

Received for publication 3 February 1978 and in revised form 20 May 1978.

REFERENCES

1. CHAPMAN, D. 1975. Phase transitions and fluidity characteristics of lipids and cell membranes. *Q. Rev. Biophys.* **8**:185.
2. MELCHIOR, D. L., and J. M. STEIM. 1976. Thermotropic transitions in biomembranes. *Annu. Rev. Biophys. Bioeng.* **5**:205.
3. DE GENNES, P. G. 1974. The Physics of Liquid Crystals. Clarendon Press, Oxford University Press, London. 347 pp.
4. LUZZATI, V., and A. TARDIEU. 1974. Lipid phases: structure and structural transitions. *Annu. Rev. Phys. Chem.* **25**:79.
5. SMALL, D. M. 1967. Phase equilibria and structure of dry and hydrated egg lecithin. *J. Lipid Res.* **8**: 551.
6. JANIAK, M. J., D. M. SMALL, and G. G. SHIPLEY. 1976. Nature of the thermal pretransition of synthetic phospholipids, dimyristoyl and dipalmitoyl-lecithin. *Biochemistry*. **15**:4575.
7. POWERS, L., and P. S. PERSHAN. 1977. Monodomain Samples of Dipalmitoyl Phosphatidylcholine with Varying Concentration of Water and Other Ingredients. *Biophys. J.* **20**:137.
8. BROCHARD, F., and P. G. DE GENNES. 1975. Hydrodynamic properties of fluid lamella phases of lipid-water. *Pramana.* Suppl. No. 1, 1.
9. POHL, D. W., S. E. SCHWARZ, and V. IRNIGER. 1973. Forced Rayleigh Scattering. *Phys. Rev. Lett.* **31**:32.
10. POHL, D. W., and v . IRNIGER. 1976. Observation of second sound in NaF by means of light scattering. *Phys. Rev. Lett.* **36**:480.
11. EICHLER, H., G. SALJE, and H. STAHL. 1973. Thermal diffusion measurements using spatially periodic temperature distributions induced by laser light. *J. Appl. Phys.* **44**:5385.
12. COWEN, J. A., C. ALLAIN, and P. LALLEMAND. 1976. Study of thermally induced light scattering in a relaxing fluid. *J. Phys. (Paris) Lett.* **37**:313.
13. MARTIN, P. C., O. PARODI, and P. S. PERSHAN. 1972. Unified hydrodynamic theory of crystals, liquid crystals and normal fluids. *Phys. Rev.* **A6**:2401.
14. TARDIEU, A., V. LUZZATI, and F. C. REMAN. 1973. Structure and polymorphism of the hydrocarbon chains of lipids: a study of lecithin-water phases. *J. Mol. Biol.* **75**:711.
15. CUMMINS, H. Z., and E. R. PIKE, editors. 1974. Photon Correlation and Light Beating Spectroscopy. Plenum Publishing Corporation, New York. 583 pp.
16. POWERS, L., and N. A. CLARK. 1972. Preparation of large monodomain phospholipid bilayer smectic liquid crystals. *Proc. Natl. Acad. Sci. U.S.A.* **72**:840.
17. MARCH, J. 1968. Advanced Organic Chemistry; Reactions, Mechanisms and Structure. McGraw-Hill Book Company, New York. 1098 pp.

18. EULER, H. V., P. KARRER, and M. RYDBOM. 1929. Uber die beziehungenzwischen A-vitaminen and carotinoiden. *Ber. Dtsch. Chem. Ges. B.* **62**:2445.
19. WILLSTATTER, R., and H. H. ESCHER. 1916. Uber den farbstoff der tomate. *Z. Physiol. Chem.* **64**:47.
20. KARRER, P., and E. JUCKER. 1950. Carotenoids. Elsevier North-Holland, Inc., New York. 350.
21. CLARK, N. A., and R. B. MEYER. 1973. Strain-induced instability of monodomain smectic-A and cholesteric liquid crystals. *Appl. Phys. Lett.* **26**:493.
22. DELAYE, M., R. RIBOTTA, and G. DURAND. 1973. Buckling instability of the layers in a smectic-A liquid crystal. *Phys. Lett. A.* **44A**:139.
23. ROSENBLATT, C. S., R. PINDAK, N. A. CLARK, and R. B. MEYER. 1977. The parabolic focal conic: a new smectic A defect. *J. Phys. (Paris).* **38**:1105–1115.
24. BEVINGTON, P. R. 1969. Data Reduction and Error Analysis for the Physical Sciences. McGraw-Hill Book Company, New York. 232–240.
25. ELWORTHY, P. H. 1961. The adsorption of water vapour by lecithin and lysolecithin, and the hydration of lysolecithin micelles. *J. Chem. Soc. (Lond.).* 5385.
26. ELWORTHY, P. H. 1962. Sorption studies on phosphatides, part II. sorption of water vapour by a synthetic lecithin and cephalin. *J. Chem. Soc. (Lond.).* 4897.
27. LENEVEU, D. M., R. P. RAND, V. A. PARSEGIAN, and D. GINGELL. 1977. Measurement and modification of forces between lecithin bilayers. *Biophys. J.* **18**:209.
28. PERSHAN, P. S., and J. PROST. 1975. Dislocation and impurity effects in smectic-A liquid crystals. *J. Appl. Phys.* **46**:2343.
29. WEAST, R. C., editor. 1976. CRC Handbook of Chemistry and Physics. 57th edition. CRC Press, Cleveland, Ohio. F56.
30. LANGE, Y., and C. M. GARY BOBO. 1974. Ion diffusion selectivity in lecithin-water lamellar phases. *J. Gen. Physiol.* **63**:690.
31. INGLEFIELD, P. T., K. A. LINDBLOM, and A. M. GOTTLEIB. 1976. Water binding and mobility in the phosphatidylcholine/cholesterol/water lamellar phase. *Biochem. Biophys. Acta.* **416**:196.
32. LINDBLOM, K. A. 1977. A proton magnetic resonance study of water binding and mobility in model biological membrane systems. Ph.D. thesis, Clark University, Worcester, Mass. Unpublished. 92 pp.
33. SANSON, A., M. PTAK, J. L. RIGAUD, and C. M. GARY BOBO. 1976. An ESR study of the hydration steps of lecithin multilayers. *Chem. Phys. Lipids.* **17**:445.
34. CHAPMAN, D., R. M. WILLIAMS, and B. D. LADBROOKE. 1967. Physical studies of phospholipids. VI. Thermotropic and lyotropic mesomorphisms of some 1,2-diacyl-phosphatidylcholines (lecithins). *Chem. Phys. Lipids.* **1**:445.

APPENDIX

If we assume a DPPC-water smectic-A system in which the anisotropic stresses are zero, the Gibbs free energy satisfies:

$$dG = -SdT + VdP + \mu_1 dN_1 + \mu_2 dn_2, \tag{A-1}$$

in which μ_i and N_i are the chemical potential and number of molecules of water for $i = 1$ and DPPC for $i = 2$. The weight fraction of water:

$$c = N_1 M_1/(N_1 M_1 + N_2 M_2), \tag{A-2}$$

where M_1 are the molecular masses of water ($i = 1$) and DPPC ($i = 2$). If we define a Gibbs free energy per mass of DPPC:

$$G \equiv N_2 M_2 g(T, P, c), \tag{A-3}$$

the quantity g is a function of only T, P, and c. It is straightforward to show:

$$(\partial g/\partial c)_{T,P} = \mu_1/M_1(1 - c)^2, \tag{A-4}$$

and the Gibbs-Duhem relation:

$$\left(\frac{c}{1-c}\right)\frac{1}{M_1}\left(\frac{\partial\mu_1}{\partial c}\right)_{T,P}+\frac{1}{M_2}\left(\frac{\partial\mu_2}{\partial c}\right)_{T,P}=0 \tag{A-5}$$

This is sufficient to show that:

$$(\partial\bar{\mu}/\partial c)_{T,P}=\frac{1}{M_1}\frac{1}{(1-c)}\left[\frac{\partial\mu_1}{\partial c}\right]_{T,P}, \tag{A-6}$$

where $\bar{\mu}=(\mu_1/M_1)-(\mu_2/M_2)$ is the variable that enters the diffusion relation (Eq. 10). Since:

$$\left(\frac{\partial\mu_1}{\partial c}\right)_{T,P}=\frac{N_1}{c(1-c)}\left(\frac{\partial\mu_1}{\partial N_1}\right)_{T,P,N_2}, \tag{A-7}$$

one can obtain:

$$\left(\frac{\partial\bar{\mu}}{\partial c}\right)_{T,P}=\frac{N_1}{M_1}\frac{1}{c(1-c)^2}\left(\frac{\partial\mu_1}{\partial N_1}\right)_{T,P,N_2}. \tag{A-8}$$